

Investigation of Solid-State Thermal Decomposition of Ammonia Borane Mix with Sulphonated Poly(ellagic Acid) for Hydrogen Release

Original

Investigation of Solid-State Thermal Decomposition of Ammonia Borane Mix with Sulphonated Poly(ellagic Acid) for Hydrogen Release / Astorino, C., De Nardo, E., Lettieri, S., Ferraro, G., Bartoli, M., Etzi, M., Chiodoni, A.M., Pirri, C.F., Bocchini, S.. - In: POLYMERS. - ISSN 2073-4360. - 16:24(2024). [10.3390/polym16243471]

Availability:

This version is available at: 11583/3003391 since: 2025-09-26T12:27:53Z

Publisher:

Multidisciplinary Digital Publishing Institute (MDPI)

Published

DOI:10.3390/polym16243471

Terms of use:

This article is made available under terms and conditions as specified in the corresponding bibliographic description in the repository

Publisher copyright

(Article begins on next page)

Article

Investigation of Solid-State Thermal Decomposition of Ammonia Borane Mix with Sulphonated Poly(ellagic Acid) for Hydrogen Release

Carmela Astorino^{1,2}, Eugenio De Nardo^{1,2}, Stefania Lettieri^{1,2,*}, Giuseppe Ferraro^{1,2}, Mattia Bartoli^{1,3,*}, Marco Etzi¹, Angelica Monica Chiodoni¹, Candido Fabrizio Pirri^{1,2} and Sergio Bocchini^{1,2}

- ¹ Center for Sustainable Future Technologies—CSFT@POLITO, Via Livorno 60, 10144 Torino, Italy; carmela.astorino@polito.it (C.A.); eugenio.denardo@polito.it (E.D.N.); giuseppe.ferraro@polito.it (G.F.); marco.etzi@iit.it (M.E.); angelica.chiodoni@iit.it (A.M.C.); fabrizio.pirri@polito.it (C.F.P.); sergio.bocchini@polito.it (S.B.)
- ² Department of Applied Science and Technology, Politecnico di Torino, C.so Duca degli Abruzzi 24, 10129 Turin, Italy
- ³ Consorzio Interuniversitario Nazionale per la Scienza e Tecnologia dei Materiali (INSTM), Via G. Giusti 9, 50121 Florence, Italy
- * Correspondence: stefania.lettieri@polito.it (S.L.); mattia.bartoli@iit.it (M.B.); Tel.: +39-0110904256 (S.L.); +39-01122918 (M.B.)

Abstract: The utilization of hydrogen in safety conditions is crucial for the development of a hydrogen-based economy. Among all methodologies, solid-state hydrogen release from ammonia borane through thermal stimuli is very promising due to the high theoretical hydrogen release. Generally, carbonaceous or inorganic matrices have been used to tune the reactivity of ammonia borane. Nevertheless, these solutions lack chemical tunability, and they do not allow one to properly tune the complex chemical pathway of hydrogen release from ammonia borane. In this study, we investigated the effect of a bioderived multifunctional polymeric matrix on hydrogen release from ammonia borane, reaching pure hydrogen release of 1.2 wt.% at 94 °C. We also describe new chemical pathways involving the formation of anchored intermediates, namely BxNy species.

Keywords: ammonia borane; hydrogen storage; bioderived polymers; ellagic acid



Citation: Astorino, C.; De Nardo, E.; Lettieri, S.; Ferraro, G.; Bartoli, M.; Etzi, M.; Chiodoni, A.M.; Pirri, C.F.; Bocchini, S. Investigation of Solid-State Thermal Decomposition of Ammonia Borane Mix with Sulphonated Poly(ellagic Acid) for Hydrogen Release. *Polymers* **2024**, *16*, 3471. <https://doi.org/10.3390/polym16243471>

Academic Editor: Jui-Ming Yeh

Received: 21 October 2024

Revised: 6 December 2024

Accepted: 10 December 2024

Published: 12 December 2024



Copyright: © 2024 by the authors. Licensee MDPI, Basel, Switzerland. This article is an open access article distributed under the terms and conditions of the Creative Commons Attribution (CC BY) license (<https://creativecommons.org/licenses/by/4.0/>).

1. Introduction

The exploration of naturally derived building blocks in polymer synthesis is primarily driven by the pursuit of environmentally sustainable, biodegradable, and less toxic materials, with a focus on leveraging nature's diversity for innovative and enhanced material properties, in response to both regulatory demands and consumer preferences for environmentally friendly products [1,2]. Their versatile properties, such as high mechanical strength, flexibility, and tunable chemical structures, make polymers an ideal platform for the development of innovative materials with a wide array of applications [3–5]. Polymers that blend favorable attributes obtained from aromatic rings (such as superior mechanical and thermal properties) with the potential for post-reactions or post-functionalization offer a wide range of opportunities for various applications [6,7]. Ellagic acid (EA) is a naturally occurring polyphenolic compound, abundantly found in several fruits and nuts, such as strawberries, pomegranates, and walnuts [8–11]. EA has attracted considerable attention in recent years, particularly for its remarkable antioxidant, anticancer, and anti-inflammatory properties, making it a promising candidate for biomedical applications [12–14]. It can be extracted from natural sources, although several studies have reported its synthesis [9] and functionalization even at a large scale [15,16]. The chemical structure of EA is unusual, comprising two gallic acid units connected by a central glucose molecule, resulting in a dimeric structure known as ellagitannin. The presence of multiple hydroxyl groups on the

phenolic rings provides ample sites for chemical modification, facilitating the synthesis of various polymer architectures and enhancing the functionality of materials based on EA. Beyond food and biomedical applications, EA could represent a particularly interesting feedstock for the production of multifunctional polymers. To the best of our knowledge, a copolymer of a first-generation polymer of intrinsic microporosity (PIM-1) and EA, which represents the sole published instance of an EA-based polymer (PEA), has been reported for application in gas separation processes (specifically CO₂/N₂ and CO₂/CH₄) [17]. Furthermore, the use of such multifunctional microporous PEA is also very promising as a host material for the incorporation of solid-state hydrogen carriers such as ammonia borane (AB). AB is a hydrogen-dense carrier that has achieved theoretical hydrogen release of up to 19.6 wt.% [18]. Nevertheless, the solid-state chemical reactivity of AB involves several simultaneous reaction pathways [19], while AB hydrolysis is relatively easy to perform [20], together with other green routes, such as photocatalytic degradation, using several high-performing catalysts [21–25].

The release of hydrogen-rich intermediates such as borazine or AB dimers and the regenerability of solid-state systems based on AB are the main issues to be addressed [26,27]. Entrapping the volatile intermediates and the successive reactions between them represents a very interesting approach to modulate hydrogen release from AB under thermal stimuli [28]. Commonly, AB is trapped in carbonaceous [29,30] or inorganic porous materials [31,32] to avoid this setback. Nonetheless, the common confinement routes lack in tunability of the matrix's chemical features. In the present work, we propose a new system based on an AB blend with sulfonated poly(ellagic acid) (SPEA) as a reliable tool to tune the reactivity of AB using a porous functional polymeric matrix produced from biologically abundant resources. We herein report a detailed study on the interactions between AB and SPEA by monitoring the thermal degradation using thermogravimetric analysis coupled with IR (TGA-IR), providing new insights into the system's reactivity.

2. Materials and Methods

2.1. Materials

All solvents and reagents were used as received, without further purification. EA was purchased from Biosynth (Siena, Italy). All other reagents and solvents were purchased from Merck (Sigma-Aldrich, St. Louis, MO, USA).

2.2. Synthesis of SPEA, AB, and AB@SPEA

The reaction was carried out according to the scheme reported in the Supporting Information (Figure S1). A mixture of anhydrous K₂CO₃ (4.5 eq, 5.53 g), EA (1 eq, 2.66 g), and 2,3,5,6-tetrafluoroterephthalonitrile (1 eq, 1.76 g) in dry N-methylpyrrolidone (30 mL) was stirred at 65 °C for 24 h under N₂, adapting the procedure reported by Hossain et al. [17]. A whitish precipitate was formed and then washed several times with fresh methanol. The as-obtained PEA was dried overnight under a vacuum. Then, 1.2 g of PEA was stirred overnight at room temperature (RT) in 20 mL H₂SO₄. The as-obtained SPEA was then precipitated in distilled water and washed several times until a neutral pH in the washing water was obtained.

AB was produced as reported by Ramachandran et al. [33]; briefly, sodium borohydride (1 eq, 3.78 g) and ammonium sulfate (1 eq, 13.21 g) were mixed at 40 °C in tetrahydrofuran for 3 h. The reaction mixture was filtered and the recovered solution was dried under a vacuum to obtain AB. The solid was further dried at 40 °C under a vacuum for 16 h.

AB@SPEA mixtures were prepared by dissolving 50 mg of SPEA+AB in tetrahydrofuran. Two different weight ratios of AB:SPEA were investigated: 5:1 (AB@SPEA 5) and 1:1 (AB@SPEA 1). The solutions were dried at room temperature and then under a vacuum at 40 °C overnight before further analysis.

2.3. Physicochemical Characterization of SPEA and AB@SPEA

TGA-IR analyses were carried out using a thermogravimetric analyzer, the NETZSCH TG 209 F1, connected by a transfer line heated at 230 °C with an IR Bruker TENSOR II equipped with an IR gas cell heated at 200 °C. For AB@SPEA, the tests were performed by heating ~3 mg of the sample in alumina pans from 30 to 350 °C with a rate of 10 °C min⁻¹ under a N₂ flow of 40 mL min⁻¹. For PEA and SPEA, ~10 mg of each sample was analyzed in a temperature range of 30 to 800 °C with a rate of 10 °C min⁻¹ under a N₂ flow of 40 mL min⁻¹.

Fourier-transformed IR in attenuated total reflection (FT-IR ATR mode) was employed to characterize the membranes. Measurements were carried out on a Bruker Tensor II Fourier transform spectrophotometer. The spectra were acquired by accumulating 64 scans (64 for the background spectrum) in the 500–4000 cm⁻¹ range with a resolution of 2 cm⁻¹.

Differential scanning calorimetry (DSC) was performed using a Netzsch DSC 204 F1 Phoenix instrument, equipped with a low-temperature probe. The experiments were carried out between -70 and 180 °C in a N₂ atmosphere (70 mL min⁻¹) by weighing 3 mg of each sample. The activation energy of the dehydrogenation process of AB@SPEA was calculated by using the Kissinger equation with data collected through DSC analyses using heating rates of 2, 5, and 10 °C min⁻¹.

XRD analyses were performed using a Panalytical X'PERT PRO PW3040/60 diffractometer (Cu K α radiation at 40 kV and 40 mA, Panalytical BV, Almelo, The Netherlands). The diffraction spectra were obtained from powder in the 2θ range from 15 to 60° with a step size of 0.013°. The XRD spectra were analyzed using the freeware QualX software 2.0.

3. Results

3.1. Evaluation of Dehydrogenation Activation Energy of AB@SPEAx (x = 1, 5)

The solid-state reactivity of AB is rather complex [18] due to the involvement of several degradative pathways, including the release of ammonia, boron-based species, and pure hydrogen. The release of molecular hydrogen occurs at the very early stage of AB's thermal decomposition, and it is easily visible through the DSC analysis of AB-containing samples as an exothermic peak at 90 to 110 °C, depending on the surrounding chemical environment [34,35]. The exothermic peak related to the first dehydrogenative step of AB can be used for the evaluation of the activation energy (E_a) using the non-isothermal Kissinger equation [36]:

$$\ln\left(\frac{HR}{T_p^2}\right) = \frac{-E_a}{RT_p} + \ln\left(\frac{Z}{RE_a}\right) \quad (1)$$

where R is the ideal gas constant (8.31 J mol⁻¹ K⁻¹), HR is the heating rate used (2, 5, 10 °C min⁻¹), T_p is the exothermic peak temperature in K as reported in the Supporting Information (Figure S4), E_a is the activation energy of the dehydrogenative process, and Z is a kinetic constant. E_a was evaluated by plotting ln(α/T_p²) versus 1/T_p using a linear fit, as shown in Figure 1.

As reported in Figure 1a, the Kissinger plots of AB@SPEAx (x = 1, 5) showed significant differences compared with pure AB, suggesting a relevant improvement in the kinetics of the thermal degradative process. AB dehydrogenation showed an E_a of up to 168 kJ mol⁻¹, in agreement with the previous work by Gutowska et al. [37] (E_a = 161 kJ mol⁻¹). The E_a of AB@SPEA5 showed a value of 148 kJ mol⁻¹, while the E_a of AB@SPEA1 was 112 kJ mol⁻¹. The trend of the E_a suggests a direct correlation between the decrease in the AB/SPEA ratio and AB destabilization. This is reasonable due to the destabilization of the N-B bond from the interaction with the sulfuric residues present on the SPEA chains, in agreement with the previous findings of Chandra et al. [38] regarding sulfonic acid resins.

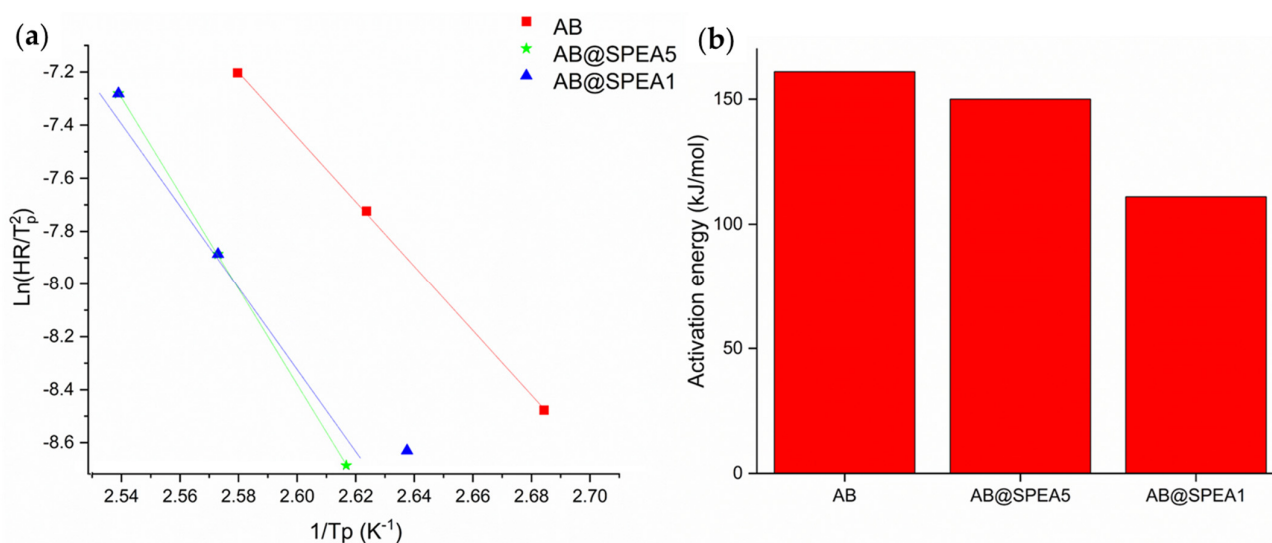


Figure 1. Data output of DSC elaboration using Kissinger equation reported as (a) Kissinger plot and (b) activation energies of AB@SPEAx (x: 1 or 5) during first dehydrogenation.

3.2. Thermal Degradative Process of AB@SPEAx (x = 1, 5)

The FT-IR SPEA spectra of all samples are reported in Figure 2. The FT-IR spectrum of AB showed a broad band composed of three components centered at three large and intense peaks at around 3178, 3247, and 3298 cm^{-1} due to ν_{NH} , while symmetric and asymmetric ν_{BH} were centered at 2382, 2316, and 2270 cm^{-1} [39]. As mentioned by Hess et al. [40], there were other two bands centered at 2426 and 2212 cm^{-1} , which cannot be attributed to a well-defined atomic vibration but to a composition of lattice vibrations. The umbrella and scissoring modes of $-\text{NH}_3$ occurred at 1603 and 1327 cm^{-1} , while the ones related to $-\text{BH}_3$ were detected at 1186 and 1160 cm^{-1} , respectively. A split band at 1380 and 1323 cm^{-1} was due to the overtones of $-\text{NH}_3$ deformations, as previously described [40]. ρ_{BNH} was observed at 1052 cm^{-1} while the symmetric and asymmetric ν_{BN} were observed at 843 and 717 cm^{-1} , respectively. The spectrum of SPEA showed a characteristic ν_{OH} peak at 3554 cm^{-1} due to the hydroxylic terminations [41] and a broad band centered at 3077 cm^{-1} due to unsaturated ν_{CH} . The polymerization was proven by the presence of a sharp peak centered at 2245 cm^{-1} due to the nitrile ν_{CN} , while the symmetrical and asymmetrical $\nu_{\text{S=O}}$ bands were centered at 1184 and 1171 cm^{-1} , respectively, proving the sulfonation of poly(ellagic acid). The AB@SPEAx (x = 1, 5) showed the same band pattern as AB with shoulders and the broadening of the peaks due to the presence of SPEA.

A detailed degradative investigation of AB, SPEA, and AB@SPEAx (x = 1, 5) was conducted using TGA-IR with quantitative analysis based on the thermograms and FT-IR spectra reported in Figures 3 and 4, respectively, and summarized in Table 1.

Table 1. Results from TGA analyses in nitrogen for AB, SPEA, and AB@SPEAx (x = 1, 5).

Sample	T_{onset} ($^{\circ}\text{C}$)	T_{max1} ($^{\circ}\text{C}$)	Residue @ T_{max1} (%)	T_{max2} ($^{\circ}\text{C}$)	Residue @ T_{max2} (%)	Residue @ 350 $^{\circ}\text{C}$ (%)	H_2 Solo Production (wt.%) ^a
AB	105	106	93.4	162	75.1	48.0	0.23
SPEA	97	144	91.2	---	---	14.7	---
AB@SPEA1	82	118	84.2	158	75.4	75.2	1.2
AB@SPEA5	86	119	78.9	164	62.1	60.0	0.9

^a Calculated as (mass loss of AB@SPEAx (x = 1, 5) prior to the release of any IR detectable compound) - (mass loss of SPEA in the same temperature range).

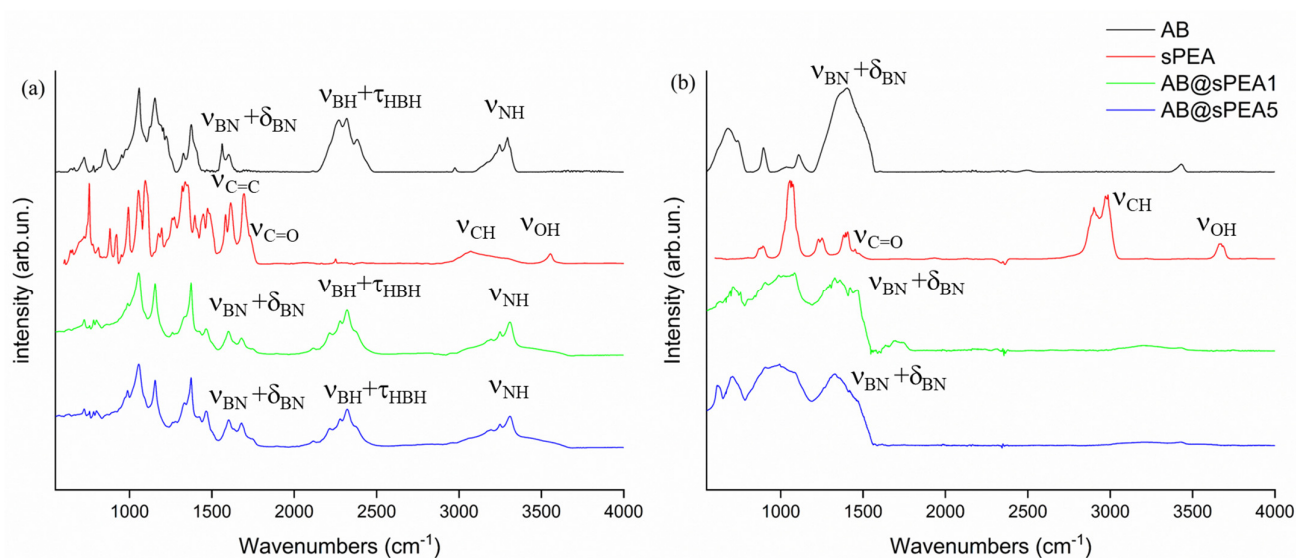


Figure 2. FT-IR spectra (ATR mode) of AB (black line), SPEA (red line), AB@sPEA1 (blue line), and AB@sPEA5 (green line) (a) pre- and (b) post-TGA-IR analysis in the range between 500 and 4000 cm^{-1} . The more relevant peaks are highlighted.

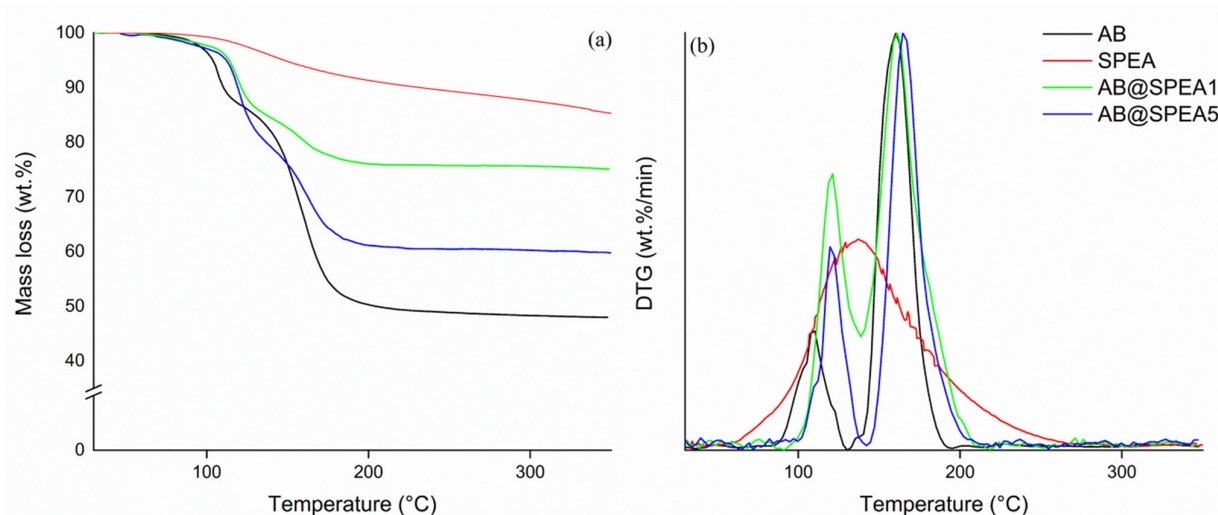


Figure 3. TGA (a) and DTG (b) of AB (black line), SPEA (red line), AB@sPEA1 (blue line), and AB@sPEA5 (green line).

The quantification of SPEA functionalization was challenging due to its poor solubility in any solvent. Nevertheless, the TGA-IR analysis of SPEA can be compared to the one run with the PEA precursors in order to evaluate the effectiveness of the sulfonation process (see Supporting Information, Figures S2 and S3). The molecular weight of SPEA was $588.44 \text{ g mol}^{-1}$, and the sulfonic residues that represented 27.6 wt.% of SPEA showed a weight loss of up to 16.8% in the range of up to 400 °C (see Supporting Information, Figure S3), while PEA lost up to 6.4 wt.%. As shown by the FT-IR spectra of the gas released during the main degradative stages of the TGA-IR analysis (see Supporting Information, Figure S4), SPEA and PEA released CO_2 and CO as a consequence of ester function degradation; moreover, SPEA released also SO_2 due to the degradation of the sulfonic residues. Accordingly, the degree of sulfonation, calculated as (mass loss of SPEA-mass loss of PEA) in the temperature range of up to 400 °C, was up to 37.7%.

AB and AB@sPEAx ($x = 1, 5$) showed major degradative steps that included several simultaneous reaction pathways, as shown in Figure 4.

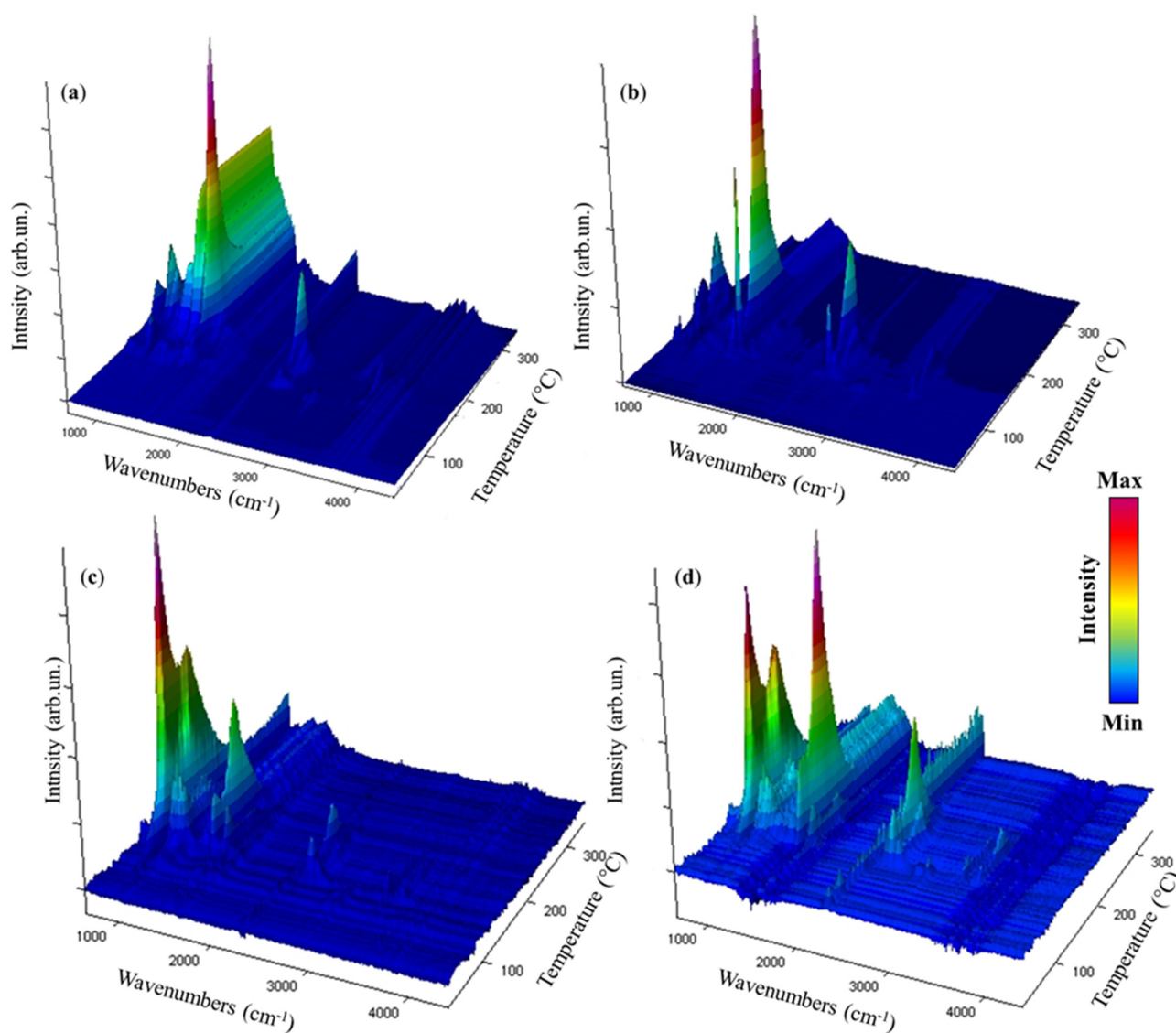


Figure 4. IR spectra collected during the thermal degradation of (a) AB, (b) SPEA, (c) AB@SPEA1, and (d) AB@SPEA5 in the temperature range of 30–350 °C.

According to Figure 4a, AB released molecular H₂ at up to 61 °C, with a mass loss of up to 0.2 wt.%, while the release of both NH₃ and B₂H₆ was confirmed by the new IR feature due to ν_{NH} at 965 cm⁻¹ and 930 cm⁻¹ [42] and diborane τ_{HBH} at 2584–2523 cm⁻¹, ν_{BH} at 2361–2329 cm⁻¹, and δ_{BH} at 1387 cm⁻¹ [43]. The presence of these species suggested an initial degradative pathway involving the cleavage of the N-B bond with the coupling of two molecules of BH₃ in the gas phase [44]. At 86 °C, we observed bands of ν_{BN} of NH₂BH₂ centered at 1392 cm⁻¹ and 1334 cm⁻¹ [45], while, at temperatures higher than 100 °C, borazine was formed, producing typical bands at 1470–1460 cm⁻¹ and 2741–2396 cm⁻¹, as described by Kaldor et al. [46]. The borazine formation reached the maximum at 162 °C, with a residue at 350 °C of up to 48.0 wt.%. AB@SPEA5 showed the release of molecular H₂ at up to 83 °C, with the gravimetric release of 0.9 wt.%. Interestingly, AB@SPEA5 released a mixture of NH₃ and B₂H₆ up to 123 °C, accordingly with the mechanism of reaction described by Al-Kukhun et al. [47]. From 123 °C onward, AB@SPEA5 released dimers of AB until 207 °C, when it released dehydrogenated borazine and NH₃. Similarly, AB@SPEA1 released pure H₂ up to 94 °C, with gravimetric release of up to 1.2 wt.%. In this case, only NH₃ was released up to 111 °C, when a degradative pathway activated the release of B₂H₆, while dehydrogenated borazine and NH₃ were released from 207 °C.

3.3. Mechanistic Insights into the Thermal Degradative Process of AB@SPEAx ($x = 1, 5$)

As shown in Figure 2b, the solid residues of AB@SPEAx ($x = 1, 5$) were considerably different compared with AB, showing a broader envelope of bands between 1565 and 1190 cm^{-1} due to ν_{BN} and δ_{BN} ; in addition, we observed, for AB@SPEA, the envelopment of the bands between 1000 and 550 cm^{-1} due to skeletal modes that were closer to the one observed for boron carbon nitride [48]. As shown in Figure 5, SPEA showed broad signals centered at 21.8° and 27.1°, while AB showed a signal pattern with peaks centered at 23.9°, 24.2°, 24.5°, 31.9°, and 34.2°, suggesting the presence of an orthorhombic phase, as reported by Hoon et al. [49]. AB@SPEA5 showed a similar pattern in which peak 020 shifted at 32.1°, with a considerable reduction in intensity, suggesting the presence of a tetragonal phase, while the broad signal of SPEA was not appreciable. This was reasonable due to the temperature treatment applied to remove the solvent used during the SPEA mixing. Interestingly, AB@SPEA5, after thermal treatment, showed XRD spectra close to the one of AB treated at more than 1500 °C, as reported by Frueh et al. [50], with four peaks centered at 16.3°, 23.3°, 29.9°, and 30.9°. This suggests the low-temperature rearrangement of the N_xB_y species formed at 350 °C during the degradation of AB.

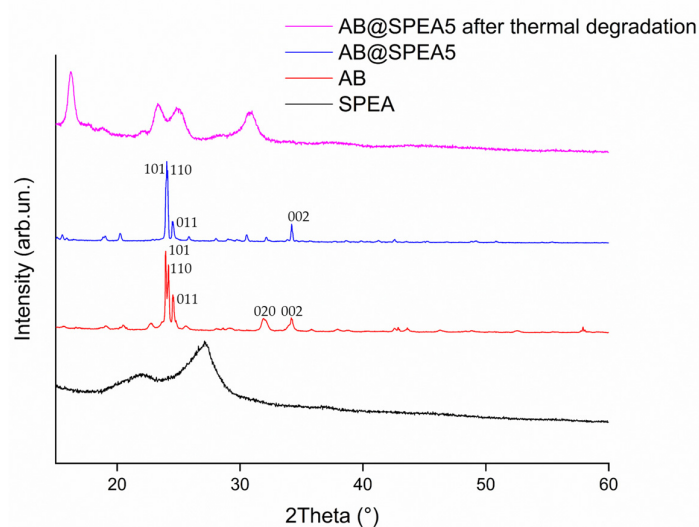


Figure 5. XRD spectra of AB, SPEA, AB@SPEA5, and AB@SPEA5 after thermal degradation.

Accordingly, we hypothesized a mechanism of degradation for AB in the presence of SPEA, as reported in Figure 6.

AB undergoes a complex degradative mechanism, moving through the formation of **1** and linear dehydrogenated B_xN_y (**3**) or through **2** with the release of borazine and a mixture of **4** and H_2 . Nevertheless, SPEA displayed several interesting reactive residues, ranging from nitriles to esters in the presence of sulfonated residues, which can act as acid catalyst sites. The reactivity of AB with these species is well known [51] and it can form intermediates such as **5** and **9** [52]. As reported by Bartoli et al. [29], borazine is generally released at temperatures higher than 100 °C, but we solely observed **4** at temperatures higher than 200 °C. This suggests that the occurrence of the reaction between borazine and reduced SPEA derivatives in the presence of acid catalysis is promoted by sulfonic residues, forming species such as **6** and **10** through nucleophilic addition reactions [53]. Furthermore, the mechanism of formation, such as the one leading to the production of **8**, explains the formation of NH_3 across the overall degradative process, with the N-terminal of anchored B_xN_y being released, reducing the formation of linear dehydrogenated species. This agrees with the IR of the residues that showed similarity with carbon boron nitride and with the release of dehydrogenated borazine. As shown in Figure 7, the Raman analysis showed the advancement of the dehydrogenation of AB with the disappearance of the ν_{BN} , while AB@SPEA5 showed the complex envelopment of the bands between 1500 and 1600 cm^{-1} .

Furthermore, the disappearance of the ν_{CN} supports the mechanism reported in Figure 5, with the anchoring steps of B_xN_y species.

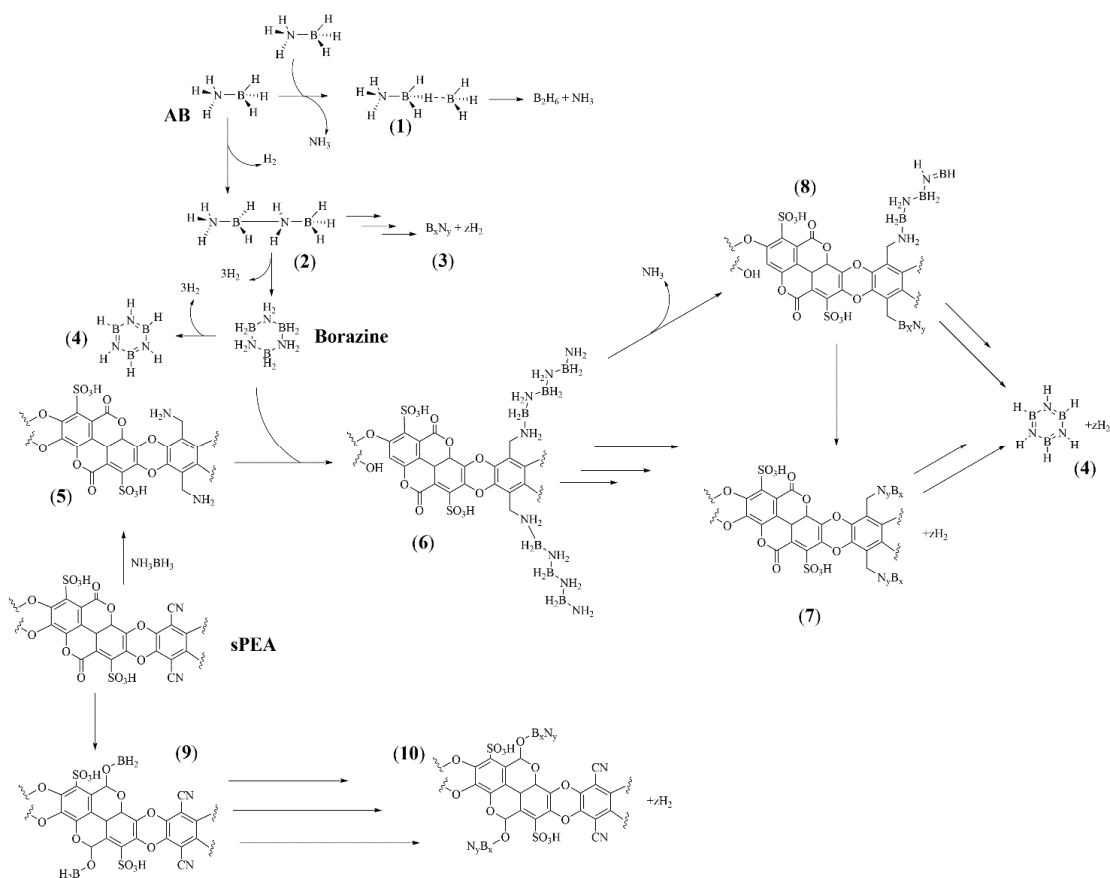


Figure 6. Hypothetical chemical pathways occurring during the thermal degradation of AB@SPEAx ($x = 1, 5$) with intermediated numbered from 1 to 10.

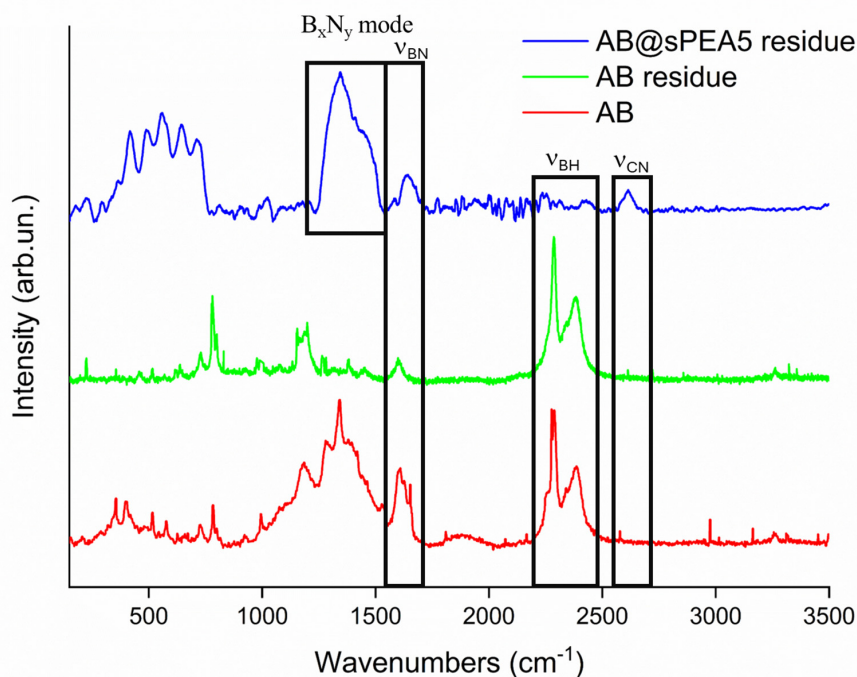


Figure 7. Raman spectra of AB, AB residue, and AB@sPEA5 in the range of 250 to 3500 cm^{-1} .

This latter species was released at temperatures higher than 200 °C, suggesting a trade-off between the length of B_xN_y and their stability.

4. Conclusions

Confinement in a specialized matrix is a well-established practice to provide a solid tool for the controlled thermal degradation of AB. In this study, we synthesized a bioderived multifunctional polymeric matrix that promoted the solid-state reaction pathways of AB by fine-tuning the AB/SPEA interaction. Accordingly, we reported hydrogen storage release up to 1.2 wt.% and the modulation of the E_a with a decrement of up to 31%. The reduction in the E_a is of particular interest due to the possibility of hydrogen release at lower temperatures, coupled with a system that is able to entrap the eventual side products produced. The hypothesized mechanism, together with the TGA-IR and FT-IR outputs, clearly shows the entrapment of volatile species on specific sites of SPEA, increasing the hydrogen mixed with B_xN_y dehydrogenated species. AB@SPEA_x (x = 1, 5) represents the first successful attempt to modulate the AB solid-state reactivity by using a polymeric matrix that is able to entrap the intermediates formed with a reduction in temperature release.

Supplementary Materials: The following supporting information can be downloaded at: <https://www.mdpi.com/article/10.3390/polym16243471/s1>, Figure S1: (a) DSC analysis of AB, (b) AB@sPEA5, and (c) AB@sPEA1 using 2, 5, and 10 °C/min as the heating rate, Figure S2: Chemical pathway for the production of SPEA using EA and 2,3,5,6-tetrafluoroterephthalonitrile as precursors, Figure S3: Thermograms of PEA and SPEA in the range of up to 800 °C in a nitrogen atmosphere; Figure S4: FT-IR spectra of gas released during the main degradative stages of PEA and sPEA in a nitrogen atmosphere during TGA-IR analysis.

Author Contributions: Conceptualization, S.L. and M.B.; methodology, S.L. and M.B.; validation, S.L., G.F., M.B., M.E. and S.B.; formal analysis, C.A., E.D.N., S.L., G.F., M.B. and M.E.; investigation, S.L., G.F., M.B., M.E., A.M.C. and S.B.; resources, C.F.P., A.M.C. and S.B.; writing—original draft preparation, C.A., E.D.N., S.L., G.F., M.B., M.E., C.F.P., A.M.C. and S.B.; writing—review and editing, C.A., E.D.N., S.L., G.F., M.B., M.E., C.F.P., A.M.C. and S.B.; visualization, C.A., E.D.N., S.L., G.F., M.B., M.E., C.F.P. and S.B.; supervision, C.F.P. and S.B.; project administration, C.F.P. and S.B.; funding acquisition, C.F.P. and S.B. All authors have read and agreed to the published version of the manuscript.

Funding: Study was carried out within the Agritech National Research Center and received funding from the European Union NextGenerationEU (PIANO NAZIONALE DI RIPRESA E RESILIENZA (PNRR)—MISSIONE 4 COMPONENTE 2, INVESTIMENTO 1.4—D.D. 1032 17 June 2022, CN00000022). Furthermore, the authors wish to thank the European Union for the financial support through the NextGenerationEU projects “Nord Ovest Digitale E Sostenibile—NODES” (PNRR, D.D. n.1054 23 June 2022), NEST “Network for Energy Sustainable Transition—NEST”(PE0000021, D.D. n.341 15 March 2022), and PNRR Mission 4 “Education and Research”—Component 2 “From research to business”—Investment 3.1 “Fund for the realization of an integrated system of research and innovation infrastructures”—Call for tender No. n. 3264 of 28/12/2021 of Italian Ministry of Research funded by the European Union—NextGenerationEU—Project code: IR0000027, Concession Decree No. 128 of 21/06/2022 adopted by the Italian Ministry of Research, CUP: B33C22000710006, Project title: iENTRANCE. The authors also acknowledge the Ministero dello Sviluppo Economico (MISE) and Ministero della Transizione Ecologica (MITE) for the financial support. This manuscript reflects only the authors’ views and opinions; neither the European Union nor the European Commission can be considered responsible for them.

Data Availability Statement: The original contributions presented in the study are included in the article/Supplementary Materials, further inquiries can be directed to the corresponding author/s.

Conflicts of Interest: The authors declare no conflicts of interest.

References

1. Fonseca, A.C.; Lima, M.S.; Sousa, A.F.; Silvestre, A.J.; Coelho, J.F.; Serra, A.C. Cinnamic acid derivatives as promising building blocks for advanced polymers: Synthesis, properties and applications. *Polym. Chem.* **2019**, *10*, 1696–1723. [[CrossRef](#)]
2. Nanni, A.; Parisi, M.; Colonna, M. Wine by-products as raw materials for the production of biopolymers and of natural reinforcing fillers: A critical review. *Polymers* **2021**, *13*, 381. [[CrossRef](#)] [[PubMed](#)]

3. Lalit, R.; Mayank, P.; Ankur, K. Natural fibers and biopolymers characterization: A future potential composite material. *Stroj. Čas.-J. Mech. Eng.* **2018**, *68*, 33–50. [[CrossRef](#)]
4. Rahman, M.Z.; Rahman, M.; Mahub, T.; Ashiquzzaman, M.; Sagadevan, S.; Hoque, M.E. Advanced biopolymers for automobile and aviation engineering applications. *J. Polym. Res.* **2023**, *30*, 106. [[CrossRef](#)]
5. Kartik, A.; Akhil, D.; Lakshmi, D.; Gopinath, K.P.; Arun, J.; Sivaramakrishnan, R.; Pugazhendhi, A. A critical review on production of biopolymers from algae biomass and their applications. *Bioresour. Technol.* **2021**, *329*, 124868. [[CrossRef](#)]
6. Thakur, M.K.; Rana, A.K.; Liping, Y.; Singha, A.S.; Thakur, V.K. Surface modification of biopolymers: An overview. *Surf. Modif. Biopolym.* **2015**, *1*, 1–19.
7. Muir, V.G.; Burdick, J.A. Chemically modified biopolymers for the formation of biomedical hydrogels. *Chem. Rev.* **2020**, *121*, 10908–10949. [[CrossRef](#)]
8. Goriparti, S.; Harish, M.; Sampath, S. Ellagic acid—a novel organic electrode material for high capacity lithium ion batteries. *Chem. Commun.* **2013**, *49*, 7234–7236. [[CrossRef](#)]
9. Evtuyugin, D.D.; Magina, S.; Evtuguin, D.V. Recent advances in the production and applications of ellagic acid and its derivatives. A review. *Molecules* **2020**, *25*, 2745. [[CrossRef](#)]
10. Wang, H.; Xu, X.; Lee, C.; Johnson, C.; Sohlberg, K.; Ji, H.-F. Highly selective sensing of nitroaromatics using nanomaterials of ellagic acid. *J. Phys. Chem. C* **2012**, *116*, 4442–4448. [[CrossRef](#)]
11. Moon, K.M.; Kwon, E.-B.; Lee, B.; Kim, C.Y. Recent trends in controlling the enzymatic browning of fruit and vegetable products. *Molecules* **2020**, *25*, 2754. [[CrossRef](#)] [[PubMed](#)]
12. Xue, P.; Zhang, G.; Zhang, J.; Ren, L. Synergism of ellagic acid in combination with radiotherapy and chemotherapy for cancer treatment. *Phytomedicine* **2022**, *99*, 153998. [[CrossRef](#)] [[PubMed](#)]
13. Aishwarya, V.; Solaipriya, S.; Sivaramakrishnan, V. Role of ellagic acid for the prevention and treatment of liver diseases. *Phytother. Res.* **2021**, *35*, 2925–2944. [[CrossRef](#)] [[PubMed](#)]
14. Bisen, P.S.; Bundela, S.S.; Sharma, A. Ellagic acid-chemopreventive role in oral cancer. *J. Cancer Sci. Ther.* **2012**, *4*, 23–30. [[CrossRef](#)]
15. Quideau, S.; Feldman, K.S. Ellagitannin chemistry. *Chem. Rev.* **1996**, *96*, 475–504. [[CrossRef](#)]
16. Yamada, H.; Wakamori, S.; Hirokane, T.; Ikeuchi, K.; Matsumoto, S. Structural revisions in natural ellagitannins. *Molecules* **2018**, *23*, 1901. [[CrossRef](#)]
17. Hossain, I.; Husna, A.; Kim, D.; Kim, T.-H. (PIM-co-Ellagic Acid)-based Copolymer Membranes for High Performance CO₂ Separation. *Membr. J.* **2020**, *30*, 420–432. [[CrossRef](#)]
18. Akbayrak, S.; Özkar, S. Ammonia borane as hydrogen storage materials. *Int. J. Hydrogen Energy* **2018**, *43*, 18592–18606. [[CrossRef](#)]
19. Demirci, U.B. Mechanistic insights into the thermal decomposition of ammonia borane, a material studied for chemical hydrogen storage. *Inorg. Chem. Front.* **2021**, *8*, 1900–1930. [[CrossRef](#)]
20. Gianola, G.; Bartoli, M.; Pirri, C.F.; Bocchini, S. Hydrogen evolution through ammonia borane hydrolysis over iron tailored pig manure catalyst. *Int. J. Hydrogen Energy* **2023**, *51*, 21–28. [[CrossRef](#)]
21. Chang, J.-P.; Wang, C.-Y.; Hsu, Y.-J.; Wang, C.-Y. Cu₂O/UiO-66-NH₂ composite photocatalysts for efficient hydrogen production from ammonia borane hydrolysis. *Appl. Catal. A Gen.* **2023**, *650*, 119005. [[CrossRef](#)]
22. Fang, M.-J.; Lin, Y.-C.; Jan, J.-Y.; Lai, T.-H.; Hsieh, P.-Y.; Kuo, M.-Y.; Chiu, Y.-H.; Tsao, C.-W.; Chen, Y.-A.; Wang, Y.-T. Au@Cu₂O core@shell nanocrystals as sustainable catalysts for efficient hydrogen production from ammonia borane. *Appl. Catal. B Environ.* **2023**, *324*, 122198. [[CrossRef](#)]
23. Liao, J.; Li, Y.; Tian, J.; Feng, Y.; Liu, Q.; Li, H. Morphology engineering of hollow core@shell structured Co₃O₄@CuO-NiO for fast hydrogen release from ammonia borane methanolysis. *J. Colloid Interface Sci.* **2024**, *680*, 78–87. [[CrossRef](#)] [[PubMed](#)]
24. Tang, S.; Xu, L.; Ding, X.; Lv, Q.; Qin, H.; Li, A.; Yang, X.; Han, J.; Song, F. Electronic engineering induced ultrafine non-noble nanoparticles for high-performance hydrogen evolution from ammonia borane hydrolysis. *Fuel* **2025**, *381*, 133424. [[CrossRef](#)]
25. Chen, Y.; Lang, Z.; Feng, K.; Wang, K.; Li, Y.; Kang, Z.; Guo, L.; Zhong, J.; Lu, J. Practical H₂ supply from ammonia borane enabled by amorphous iron domain. *Nat. Commun.* **2024**, *15*, 9113. [[CrossRef](#)] [[PubMed](#)]
26. Demirci, U.B. Ammonia borane: An extensively studied, though not yet implemented, hydrogen carrier. *Energies* **2020**, *13*, 3071. [[CrossRef](#)]
27. Shimizu, Y.; Miyagi, A.; Tripathi, A.K.; Nakagawa, T. Delayed ammonia release of ammonia borane hydrolysis by citric acid. *Int. J. Hydrogen Energy* **2024**, *82*, 733–739. [[CrossRef](#)]
28. Li, J.; Feng, Y.; Li, X.; Zhang, T.; Liu, X.; Wang, N.; Sun, Q. Sub-2 nm Ternary Metallic Alloy Encapsulated within Montmorillonite Interlayers for Efficient Hydrogen Generation from Ammonia Borane Hydrolysis. *ACS Catal.* **2024**, *14*, 14665–14677. [[CrossRef](#)]
29. Bartoli, M.; Pirri, C.F.; Bocchini, S. Unraveling the Effect of Carbon Nanotube Oxidation on Solid-State Decomposition of Ammonia Borane/Carbon Nanotube Composites. *J. Phys. Chem. C* **2022**, *126*, 16587–16594. [[CrossRef](#)]
30. Moussa, G.; Bernard, S.; Demirci, U.B.; Chiriach, R.; Miele, P. Room-temperature hydrogen release from activated carbon-confined ammonia borane. *Int. J. Hydrogen Energy* **2012**, *37*, 13437–13445. [[CrossRef](#)]
31. Li, Z.; Zhu, G.; Lu, G.; Qiu, S.; Yao, X. Ammonia borane confined by a metal–organic framework for chemical hydrogen storage: Enhancing kinetics and eliminating ammonia. *J. Am. Chem. Soc.* **2010**, *132*, 1490–1491. [[CrossRef](#)] [[PubMed](#)]
32. Rueda, M.; Sanz-Moral, L.M.; Segovia, J.J.; Martín, Á. Improvement of the kinetics of hydrogen release from ammonia borane confined in silica aerogel. *Microporous Mesoporous Mater.* **2017**, *237*, 189–200. [[CrossRef](#)]

33. Ramachandran, P.V.; Gagare, P.D. Preparation of ammonia borane in high yield and purity, methanolysis, and regeneration. *Inorg. Chem.* **2007**, *46*, 7810–7817. [[CrossRef](#)] [[PubMed](#)]
34. Sepehri, S.; Garcia, B.B.; Cao, G. Tuning dehydrogenation temperature of carbon–ammonia borane nanocomposites. *J. Mater. Chem.* **2008**, *18*, 4034–4037. [[CrossRef](#)]
35. Ergüven, H.; Kantürk Figen, A.; Pişkin, S. Ammonia borane–boron composites for hydrogen release: Thermolysis kinetics. *Energy Sources Part A Recovery Util. Environ. Eff.* **2017**, *39*, 613–617. [[CrossRef](#)]
36. Kissinger, H.E. Reaction kinetics in differential thermal analysis. *Anal. Chem.* **1957**, *29*, 1702–1706. [[CrossRef](#)]
37. Gutowska, A.; Li, L.; Shin, Y.; Wang, C.M.; Li, X.S.; Linehan, J.C.; Smith, R.S.; Kay, B.D.; Schmid, B.; Shaw, W. Nanoscaffold mediates hydrogen release and the reactivity of ammonia borane. *Angew. Chem.* **2005**, *117*, 3644–3648. [[CrossRef](#)]
38. Chandra, M.; Xu, Q. Dissociation and hydrolysis of ammonia-borane with solid acids and carbon dioxide: An efficient hydrogen generation system. *J. Power Sources* **2006**, *159*, 855–860. [[CrossRef](#)]
39. Paolone, A.; Teocoli, F.; Sanna, S.; Palumbo, O.; Autrey, T. Temperature Dependence of the Infrared Spectrum of Ammonia Borane: Librations, Rotations, and Molecular Vibrations. *J. Phys. Chem. C* **2013**, *117*, 729–734. [[CrossRef](#)]
40. Hess, N.J.; Bowden, M.E.; Parvanov, V.M.; Mundy, C.; Kathmann, S.M.; Schenter, G.K.; Autrey, T. Spectroscopic studies of the phase transition in ammonia borane: Raman spectroscopy of single crystal NH_3BH_3 as a function of temperature from 88 to 330 K. *J. Chem. Phys.* **2008**, *128*, 034508. [[CrossRef](#)]
41. Li, B.; Harich, K.; Wegiel, L.; Taylor, L.S.; Edgar, K.J. Stability and solubility enhancement of ellagic acid in cellulose ester solid dispersions. *Carbohydr. Polym.* **2013**, *92*, 1443–1450. [[CrossRef](#)] [[PubMed](#)]
42. McBride, J.; Nicholls, R. The vibration-rotation spectrum of ammonia gas. I. *J. Phys. B At. Mol. Phys.* **1972**, *5*, 408. [[CrossRef](#)]
43. Anderson, W.E.; Barker, E. The Infra-Red Absorption Spectrum of Diborane. *J. Chem. Phys.* **1950**, *18*, 698–705. [[CrossRef](#)]
44. Choi, H.Y.; Park, S.J.; Seo, D.; Baek, J.-m.; Song, H.D.; Jung, S.J.; Lee, K.J.; Kim, Y.L. Low-temperature synthesis of ammonia borane using diborane and ammonia. *Int. J. Hydrogen Energy* **2015**, *40*, 11779–11784. [[CrossRef](#)]
45. Gerry, M.; Lewis-Bevan, W.; Merer, A.; Westwood, N. The infrared spectrum of gaseous aminoborane, $\text{H}_2\text{N BH}_2$: Location of the fundamentals and rotational structure in the 4_0^1 band (BN stretching vibration at 1337 cm^{-1}). *J. Mol. Spectrosc.* **1985**, *110*, 153–163. [[CrossRef](#)]
46. Kaldor, A.; Porter, R.F. Matrix isolation study of borazine and boroxine. Vibrational analysis. *Inorg. Chem.* **1971**, *10*, 775–785. [[CrossRef](#)]
47. Al-Kukhun, A.; Hwang, H.T.; Varma, A. Mechanistic studies of ammonia borane dehydrogenation. *Int. J. Hydrogen Energy* **2013**, *38*, 169–179. [[CrossRef](#)]
48. Rivera-Tapia, E.D.; Fajardo, C.A.; Ávila-Vega, Á.J.; Ávila, C.F.; Sánchez-Arévalo, F.M.; Chango-Villacís, I.; Quiroz-Chávez, F.J.; Santoyo-Salazar, J.; Dante, R.C. Synthesis of boron carbon nitride oxide (BCNO) from urea and boric acid. *Fuller. Nanotub. Carbon. Nanostructures* **2016**, *24*, 8–12. [[CrossRef](#)]
49. Hoon, C.; Reynhardt, E.C. Molecular dynamics and structures of amine boranes of the type $\text{R}_3\text{N. BH}_3$. I. X-ray investigation of $\text{H}_3\text{N. BH}_3$ at 295K and 110K. *J. Phys. C Solid. State Phys.* **1983**, *16*, 6129. [[CrossRef](#)]
50. Frueh, S.; Kellett, R.; Mallery, C.; Molter, T.; Willis, W.S.; King'ondou, C.; Suib, S.L. Pyrolytic decomposition of ammonia borane to boron nitride. *Inorg. Chem.* **2011**, *50*, 783–792. [[CrossRef](#)]
51. Faverio, C.; Boselli, M.F.; Medici, F.; Benaglia, M. Ammonia borane as a reducing agent in organic synthesis. *Org. Biomol. Chem.* **2020**, *18*, 7789–7813. [[CrossRef](#)] [[PubMed](#)]
52. Cheng, T.; Bets, K.V.; Jakobson, B.I. Synthesis Landscapes for Ammonia Borane Chemical Vapor Deposition of h-BN and BNNT: Unraveling Reactions and Intermediates from First-Principles. *J. Am. Chem. Soc.* **2024**, *146*, 9318–9325. [[CrossRef](#)] [[PubMed](#)]
53. Lisovenko, A.S.; Timoshkin, A.Y. Donor– acceptor complexes of borazines. *Inorg. Chem.* **2010**, *49*, 10357–10369. [[CrossRef](#)] [[PubMed](#)]

Disclaimer/Publisher's Note: The statements, opinions and data contained in all publications are solely those of the individual author(s) and contributor(s) and not of MDPI and/or the editor(s). MDPI and/or the editor(s) disclaim responsibility for any injury to people or property resulting from any ideas, methods, instructions or products referred to in the content.